

# A fresh view on Henize 2-10 with VLT/NAOS-CONICA<sup>1</sup>

Rémi A. Cabanac<sup>2</sup>

*Canada-France-Hawaii Telescope*  
 65-1238 Mamalahoa Highway, Kamuela, HI 96743, USA  
 cabanac@cfht.hawaii.edu

Leonardo Vanzi

*European Southern Observatory*  
 Alonso de Cordova, 3107, casilla 19001, Vitacura, Santiago, Chile  
 and

Marc Sauvage

*CEA/DSM/DAPNIA/SAP - UMR AIM*  
 CE Saclay, 91191 Gif sur Yvette CEDEX, France

## ABSTRACT

We present high-resolution observations of Henize 2-10 in  $K_S$  ( $2.2\ \mu\text{m}$ ),  $L'$  ( $3.8\ \mu\text{m}$ ),  $M'$  ( $4.8\ \mu\text{m}$ ) bands. These allow for the first time to track accurately the structures at the heart of the galaxy from the optical to the radio. All radio knots previously observed can now be associated with  $L'$  and  $K_S$  emitting regions. This implies a revision of their physical nature. Instead of highly extinguished ultra-dense HII regions, we propose that two of the 5 radio knots are either supernova remnants or *normal* HII regions, while the remaining three are bona fide ultra-dense HII regions, although less obscured than was previously thought.

*Subject headings:* galaxies: individual (Henize 2-10)

## 1. Introduction

Henize 2-10 (He 2-10) is a blue compact galaxy with quite interesting properties. It is a nearby starburst galaxy with a heliocentric distance of  $9 \pm 5$  Mpc (Johansson 1987; Tully 1988). In this paper we adopt a distance of  $9\ h^{-1}\text{Mpc}$ , with  $H_0 = 75$  km/s, which yields a scale of  $\sim 45\text{pc/arcsec}$ . The galaxy shows spectroscopic Wolf-Rayet features which indicates the presence of a very young starburst region (Hutsemekers

& Surdej 1984; Vacca & Conti 1992), and has a slightly sub-solar metallicity (Kobulnicky et al. 1999). Figure 1 shows a RGB-composite image (in color in electronic version only) of the central  $18'' \times 27''$  ( $800 \times 1200$  parsecs) of He 2-10, where most of the current star formation occur. The blue and green channels are  $0.3''$ -convolved HST WFPC archive in  $F555W$  and  $F814W$ . The red channel is our  $0.3''$ -seeing  $K_S$  taken with VLT/ISAAC. The bright central nucleus, generally referred to as region A, is an arc of UV-bright super-star clusters (Vacca & Conti 1992). It is surrounded by two presumably older star-forming regions. Region B on the east shows a mixed population of blue and red clusters (only detected in  $K_S$  and longer wavelength bands). Region C,

<sup>1</sup>based on observations made at the ESO VLT under program 71.B-0492, and 270.B-5011

<sup>2</sup>also at Dep. de Astronomía y Astrofísica, Pontificia Universidad Católica de Chile, Campus San Joaquín, Vicuña Mackenna 4860, Casilla 306, Santiago 22, Chile, and Visiting scientist at ESO, Santiago

on the north-west side, has a long tail containing bright red clusters as well. Dust is clearly apparent in this image, as shown by the red filaments observed to the south-east side between A and B. These appear to be blown away from the central region, rapidly dissolving in He 2-10's interstellar medium. Assuming for the dust clouds a velocity equal to the typical sound speed in the ISM, i.e.  $10 \sim 10 \text{ km}\cdot\text{s}^{-1}$ , hence a growing rate of  $\sim 10 \text{ pc}/\text{Myr}$ , the present radii of curvature of the filaments  $\sim 50 - 100 \text{ pc}$  yield dynamical ages of  $5 - 10 \text{ Myr}$ . Region A is also flanked by two compact red sources that are only visible at  $K_S$  and longer wavelengths. These two sources get brighter with longer wavelengths, as shown in Figure 3. The various colors of the sources hint at a highly heterogeneous dust content, and possibly age differences among the cluster population.

Recent observations in the optical, IR, and radio, have brought new exciting facts.

First, the youth of the starburst event in the center was confirmed by STIS analysis of the brightest UV/optical knots by Chandar et al. (2003) which yielded a coeval formation age of 4-5 Myr for all optical clusters.

Second, the presence and importance of dust in the central region was confirmed by high-resolution mid-infrared observations (Sauvage et al. 1997; Beck et al. 2001; Vacca et al. 2002): the majority (60%) of the MIR emission is confined to a  $\sim 5''$  region, compatible in size with the location of the observed starburst. However the intrinsically large uncertainties in MIR astrometry prevented a clear identification of the MIR sources.

Finally, the radio observations of Kobulnicky & Johnson (1999, 2000) evidenced 5 compact radio sources (hereafter called the radio knots) characterized by mostly thermal spectra. The striking morphological resemblance between the radio knots and the MIR emission allowed to tie down the location of the MIR sources precisely (Beck et al. 2001). Furthermore, comparing with HST images, Kobulnicky & Johnson (1999, 2000) argued that most of these radio-MIR sources were off-centered, in the dusty area between region A and B. They thus attributed this emission to young ( $1 < \text{Myr}$ ) ultra dense (UD) HII regions with ongoing star formation hidden in dense molecular clouds. Following this interpretation, Beck et al.

(2001), from  $11.7 \mu\text{m}$  observations, derived that up to  $10^4$  O7V stars (equivalent to  $10^{49}$  Lyman photons $\cdot\text{s}^{-1}$ ) must be hidden in these dense cocoons, and Vacca et al. (2002), from  $10.8 \mu\text{m}$  observations, computed that  $10^7 M_\odot$  of dust and gas must be surrounding the UD HII regions and estimated the bolometric luminosity of the brightest MIR region overlapping with radio knot 4 to be as much as  $2 \times 10^9 L_\odot$ . Johnson & Kobulnicky (2003) extended the radio observations and refined the measurement of physical properties of the UD HII regions, in particular an anomalous low mass HII content of  $2-8 \times 10^3 M_\odot$  was found, attributed to the extreme youth of the objects.

Therefore, as of today, He 2-10 appears as a spectacular case of a starburst galaxy where a large fraction of its most current star formation activity lies completely buried in dust, and has absolutely no visible counterpart.

We present here high-resolution observations in  $K_S$  ( $2.2 \mu\text{m}$ ) with VLT/ISAAC (under ESO program 270.B-5011(A)),  $L'$  ( $3.8 \mu\text{m}$ ), and  $M'$  ( $4.8 \mu\text{m}$ ) bands with the Adaptive Optics VLT / NAOS-CONICA (under ESO program 71.B-0492(A)) that give the highest resolution to date of the nucleus of He 2-10 in the NIR, a wavelength regime adequately located between the stellar optical regime and the dust thermal regime. The high quality of the observations allows the identification, for the first time, of bright  $L'$  regions which correlate with radio knots (Kobulnicky & Johnson 1999), and  $K_S$  regions that correlate with the optically bright cluster, thus bridging the existing wavelength gap.

## 2. Observations and data reduction

We observed He 2-10 in  $K_S$  using ISAAC at the ESO VLT/Antu under  $0.3''$  seeing (Figure 1), and in  $L'$  and  $M'$  with the adaptive optics system NAOS-CONICA at the ESO VLT/Yepun, reaching a corrected PSF full width at half maximum (FWHM) of  $0.12''$ . The observations were obtained in service mode in 2003-2004. We used standard observing strategies. In  $L'$ , we alternated exposures between the object and the sky in 15 ABBA sequences with a throw of  $40''$ . Object cubes (respectively sky cubes) consisted of 220 (110) random  $0.175 \text{ s}$  jitter for a total exposure time of  $1155 \text{ s}$  ( $577.5 \text{ s}$ ). In  $M'$ , as NACO was still



Fig. 1.— He 2-10 is shown in a RGB composite image (in color in the electronic version only) of  $18'' \times 27''$  ( $800 \times 1200$  pc at a distance of 9 Mpc). North is up and East is left. The blue and green channels are  $0.3''$ -convolved HST WFPC archive images in  $F555W$  and  $F814W$ . The red channel is a  $0.3''$ -seeing  $K_S$  image taken with VLT/ISAAC. The red filaments correspond to absorption regions in HST images, hence appear red by contrast. The region on the left shows a mix of bluish clusters and red clusters, hinting at a highly heterogeneous dust content, and possibly age differences. The bright red sources on each side of the nucleus are detected only from  $K_S$  and up to radio bands (cf. text).

in early operation, we used the only allowed chopping mode with pre-defined exposure time and a 30'' chopping throw. Typical strehl ratios of validated exposures were in the range 20-25% for both filters.

The ABBA sequences were combined/subtracted using custom iraf scripts. We performed accurate astrometry reconstruction and photometry as described in the following sections.

## 2.1. Astrometry

In order to compare the astrometry of our NAOS-CONICA images with previous multiwaveband observations, we performed an accurate calibration of the NAOS-CONICA to the USNO-B based J2000 epoch. We first calibrated the astrometry of the  $K_S$  image using 23 field stars catalogued in the USNO-B (Monet et al. 1998), and applied general transformations using the NOAO iraf routine geomap. The positional accuracies of the transformations are  $\Delta\alpha_{rms} = 0.008$ sec and  $\Delta\delta_{rms} = 0.08''$ . We then derived the transformations between the  $K_S$  USNO-calibrated image and  $L$  image using four common sources in the central region (two field stars and two bright clusters). The number of available common sources is too small to derive a robust general transformation but the clear morphological similarities between the  $K_S$  and  $L$  images (Figure 3) make us confident that the reconstructed  $L$  astrometry has an accuracy equivalent to that of the  $K_S$  image. The positional accuracies of the transformations are  $\Delta\alpha_{rms} = 0.001$ sec and  $\Delta\delta_{rms} = 0.012''$ . The resulting astrometry, computed for all  $L'$  sources, is shown Table 1.

## 2.2. Photometry

We extracted  $L'$ - and  $M'$  fluxes of all detected sources of the inner core of He2-10 in aperture sizes of 0.5'' (the finding chart in  $L'$  is given Figure 2, left panel), the good match between VLT-NACO and HST resolutions allows us to compute consistent aperture photometry over the entire optical and near-infrared (NIR) range. We measured the  $F555W$ ,  $H\alpha$ ,  $F814W$  fluxes from the HST calibrated archive images, on the same positions and aperture sizes, including a systematic centroid position mismatch in the error computation. All photometric measure-

ments were then calibrated to Vega magnitudes using IR standards provided by ESO service observing team. All ancillary data may be found in [http://archive.eso.org/eso/eso\\_archive\\_main.html](http://archive.eso.org/eso/eso_archive_main.html), under Program ID 71.B-0492(A). Typically,  $L'$  errors on zeropoints are ca. 10%, because of a highly variable background. Additional uncertainties are due to the anisoplanetism of the FOV of view and the different strehl ratio between the photometric standard and the science observations. Both effect are difficult to quantify, but we assume that, because of our large apertures ( $5\times$ FWHM), the strehl difference will not dominate the systematics and most of the error will actually come from background subtraction. Unfortunately NACO's response was not fully known when the  $M'$  data were taken and the standard stars were observed with high ADU counts. They possibly reach the non-linear regime of the detector and the derived zero-points from different nights disagree to  $\pm 0.25$  mag. Hence the  $M'$  data are mostly useful for morphology and only deliver a crude photometry.

HST  $F555W$ ,  $F658N/H\alpha$ , and  $F814W$  images were analysed following standard recipes detailed by Holtzman et al. (1995). We extracted the sources of the nucleus with the full-resolution images in order to compare with  $L'$  data, and we convolved the HST data with a 0.3'' gaussian in order to compare with  $K_S$  data. We derived  $H\alpha$  equivalent width interpolating the continuum between  $F555W$  and  $F814W$  following Johnson et al. (2000). We recover the original magnitudes and similar  $H\alpha$  equivalent widths of Johnson et al. (2000) and the V magnitude of knot 4 (Chandar et al. 2003) using different strategies with smaller apertures within photon and aperture position errors.

All Vega calibrated magnitudes were corrected for the galactic extinction of  $E(B - V) = 0.11$  (Schlegel et al. 1998) yielding  $A_V = 0.369$ ,  $A_{H\alpha} = 0.298$ ,  $A_I = 0.216$ ,  $A_K = 0.04$ ,  $A_L = 0.017$ , and  $A_M = 0.0$ .

We also extracted all sources detected in  $K_S$ ,  $F814W$  and  $F555W$  in the outer 1' of He2-10 (0.5'' aperture size, see Figure 2 right panel). A special care was taken to check the effect of the larger PSF in  $K_S$  and HST convolved resolution, compared to HST original resolution. We computed the total flux lost between unconvolved and

TABLE 1  
HE 2-10: ASTROMETRY OF THE  $L'$  BRIGHT SOURCES OF THE NUCLEUS (FIG. 2)

Name <sup>a</sup> Band $L'$	R.A. (J2000) h min sec $\pm 0.003\text{sec}$	Dec. (J2000) ° ' " $\pm 0.02\text{sec}$	Name <sup>b</sup> Band 2 cm	R.A. (J2000) h min sec $\pm 0.007\text{sec}$	Dec. (J2000) ° ' " $\pm 0.1\text{sec}$
L1	8 36 15.032	-26 24 33.90	knot 1	8 36 15.014	-26 24 33.81
L2	8 36 15.066	-26 24 34.03	knot 2	8 36 15.060	-26 24 33.98
L3a	8 36 15.131	-26 24 34.24	knot 3	8 36 15.127	-26 24 34.13
L3b	8 36 15.153	-26 24 34.10	knot 3	8 36 15.127	-26 24 34.13
L4a	8 36 15.218	-26 24 34.00	knot 4	8 36 15.234	-26 24 34.00
L4b	8 36 15.247	-26 24 34.35	knot 4	8 36 15.234	-26 24 34.00
L4c	8 36 15.251	-26 24 34.83	knot 4	8 36 15.234	-26 24 34.00
L4d	8 36 15.265	-26 24 34.39	knot 4	8 36 15.234	-26 24 34.00
L5	8 36 15.310	-26 24 35.11	knot 5	8 36 15.308	-26 24 34.61
L6	8 36 15.183	-26 24 34.06			
L7	8 36 15.191	-26 24 34.60			
L8	8 36 15.217	-26 24 34.50			

<sup>a</sup>FWHM 0.12" (This work).

<sup>b</sup>Beam size  $\sim 0.4'' \times 0.8''$  (Kobulnicky & Johnson (1999, Table 3)). The astrometry is from Kobulnicky & Johnson (1999).

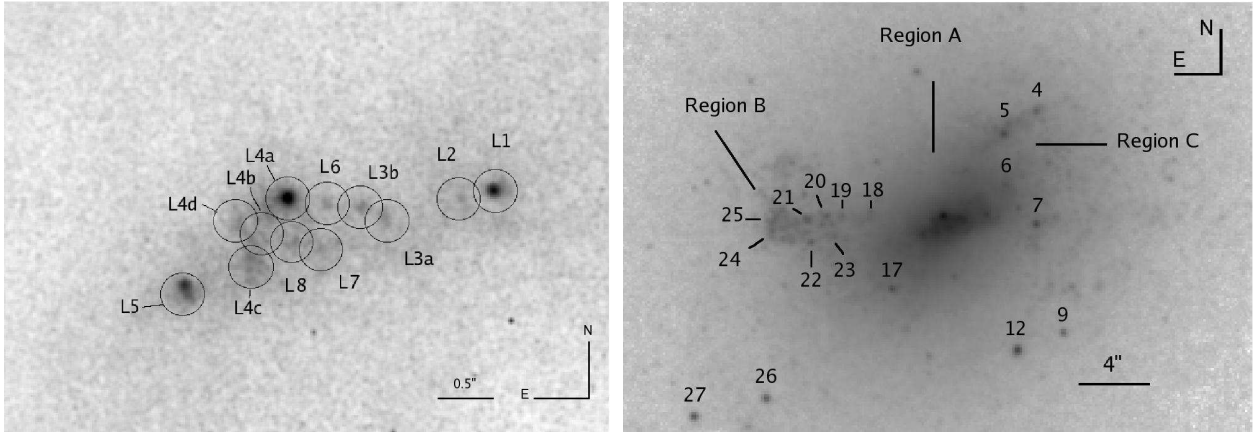


Fig. 2.— Left: He 2-10 nucleus is shown in  $L'$ , with VLT/NAOS-CONICA, FWHM 0.12 arcsec, Field of view  $\sim 7''$ , with labels referring to the source naming convention used in this paper. The apertures are 0.5" wide, or 22.5 pc at 9 Mpc. Right: He 2-10 is shown in  $K_s$  + finding chart of outer source with  $M_V < -6.5$  detected in  $V$ ,  $I$ , &  $K_s$ . Source 18 to 25 belong to region B, sources 4 to 7 to region C.

convolved point sources for  $0.5''$  apertures. The loss amounts to  $0.31 \pm 0.05$  mag in  $F814W$  and  $F555W$ . Although substantial in absolute, the correction is negligible in color, hence the color-color diagrams are not affected by the correction applied to the sources of the outer  $1'$ .

Finally, another photometric extraction was done on the brightest  $L'$  and  $M'$  sources in order to build the full spectral energy distributions of these regions. We convolved  $L'$  and  $M'$  images with  $0.3''$  and extracted fluxes around the brightest radio knots in  $1''$  apertures.

The largest source of uncertainty comes from the diffuse background in the inner core of He 2-10. We adopted different strategies to estimate the background in the different bands, in order to account for the variable resolutions and field crowding of the data. The HST images were sky subtracted using sky annuli of radius  $0.3$ - $0.5''$  around the objects located in the inner  $10''$  of the nucleus, and using annuli  $0.4$ - $0.6$  pix for outer sources (also for  $K_S$ ). In  $K_S$ ,  $L'$  and  $M'$ , we computed the diffuse emission background in annuli of radius  $0.3$ - $1''$  around the objects located in the inner  $10''$  of the nucleus. We additionally computed 2 sky annuli ( $0.3$ - $0.5''$ , and  $0.3$ - $2''$ ) in order to estimate the systematic errors resulting from the measured flux differences. Systematic errors of  $0.15$  mag were typical. The  $M'$  magnitudes have higher systematics due the uncertainty on the zeropoints. Finally the background around the  $1''$  apertures was measured in annuli of  $0.5$ - $1.5''$ .

### 3. Results

#### 3.1. Optical to radio identification of the central sources

Figure 3 shows the entire series of high-resolution observations of the nucleus of Henize 2-10, in  $F555W$ ,  $F658N/H\alpha$ ,  $F814W$ ,  $K_S$ ,  $L'$ ,  $M'$  (shifted to USNO-B absolute astrometry, see section 2.1),  $N$  and 2 cm. The  $M'$  image is much shallower than the  $L'$  image, and only the three reddest sources are robustly detected. As is evident from this figure, and also from Table 1, the  $L'$  and  $M'$  sources are clear counterparts to some of the radio knots, and because of the strong morphological and physical association between the radio and MIR emissions, to the MIR sources as well. Figure 4 shows a precise comparison of the

$L'$  images (gray scale) with  $N$  GEMINI/OSCIR  $N$  contours (left, the  $N$  source associations to the radio knots are according to Vacca et al. 2002), and with VLA 2-cm contours (right, with the radio knots identification of Kobulnicky & Johnson 1999). It is striking to see, on Fig 4, how well sources L1 and L5 correlate with the N-band sources. Furthermore Figure 3 also demonstrates the association of L4a with the brightest source in  $F814W$ , and of L6, L3a and L3b with the string of three clusters detected west of the brightest source in  $F814W$ . Therefore, in contrast to the statement of Kobulnicky & Johnson (1999, 2000), we see a clear connection between the structures observed from  $0.5 \mu\text{m}$  to 2 cm.

At this stage it is important to stress that the positional association from the optical to the radio that we present here is not a new proposition that we are making, but is a fact imposed by the astrometry. The HST,  $K_S$ ,  $L'$ , and  $M'$  images are now tied to the same astrometric reference, which is the USNO-B astrometry. This is accurate to  $\pm 0.3''$  which will be the dominant positional uncertainty in this wavelength regime (for instance the relative astrometric accuracy of NAOS-CONICA is  $\pm 0.02''$ ). The absolute astrometry of the VLA is accurate to  $\pm 0.1''$ . With these accuracies, it becomes impossible to accept the relative positions of the HST and MIR/radio sources as presented in Kobulnicky & Johnson (1999, 2000); Vacca et al. (2002), i.e. a shift of  $1.2''$  in  $\alpha$ , even taking into account the beam size of the VLA, which is  $0.4''$  in  $\alpha$ . In fact, the main source of astrometric error in previous papers was an incorrect astrometry in the HST data used at the time. This is now corrected in the archived versions of the same data. Therefore Figure 3 now reveals for the first time the correct evolution of the central region of He 2-10 from the optical to the radio. This allows now to present a much firmer identification of the different components across the spectrum.

L1 is clearly detected in  $M'$  and can now be associated to the western N band source. It has a rather faint counterpart in  $K_S$  and is no longer detected in the optical bands, and shows a clear anti-correlation with  $H\alpha$  (Fig. 5). Figure 4 shows that L1 appears to fall between the radio knots 1 and 2, however this time the shift is too small to be significant. Since L1 is accompanied by a

TABLE 2  
0.5'' APERTURE PHOTOMETRY OF HE 2-10 (FIG. 2)

Source #	$F555W$ Vega	$F814W$ Vega	$K_S$ Vega	$L'$ Vega	$\log(\text{EW}[\text{H}\alpha])$ $\log(\text{\AA})$
L1	19.48±0.08	18.53±0.06	15.61±0.03	13.53±0.01	2.60
L2	19.21±0.05	18.36±0.04	15.80±0.02	14.09±0.90	2.66
L3a	16.94±0.07	16.53±0.07	14.79±0.08	14.07±0.01	1.39
L3b	16.61±0.03	16.19±0.02	14.53±0.03	14.08±0.03	0.74
L4a	16.16±0.04	15.77±0.03	13.92±0.03	13.04±0.04	1.69
L4b	16.68±0.02	16.38±0.01	14.65±0.02	13.49±0.01	2.32
L4c	16.71±0.05	16.38±0.03	14.76±0.04	13.48±0.02	2.39
L4d	17.62±0.17	17.06±0.13	15.06±0.13	13.78±0.08	2.38
L5	18.99±0.17	18.14±0.14	15.29±0.06	13.34±0.02	2.37
L6	16.65±0.02	16.30±0.02	14.55±0.02	14.10±0.06	1.23
L7	17.67±0.04	17.04±0.03	14.75±0.02	13.83±0.02	2.21
L8	17.26±0.03	16.77±0.03	14.64±0.02	13.68±0.02	2.28

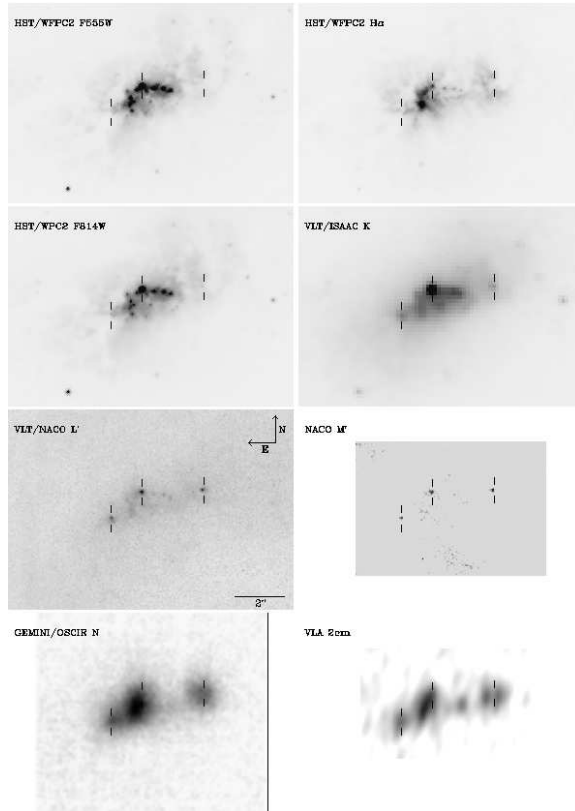


Fig. 3.— The nucleus of He 2-10 is shown from blue to radio wavelengths, from top-left to bottom-right. Each panel shows the central region observed with VLT/NAOS-CONICA in  $L'$ -band. Three bright regions are gradually emerging from the dust from  $K_S$  to radio bands. All images are now plotted on a common, identical, astrometric grid, the vertical markers replicate the position of the brightest  $L'$  sources in all panels.

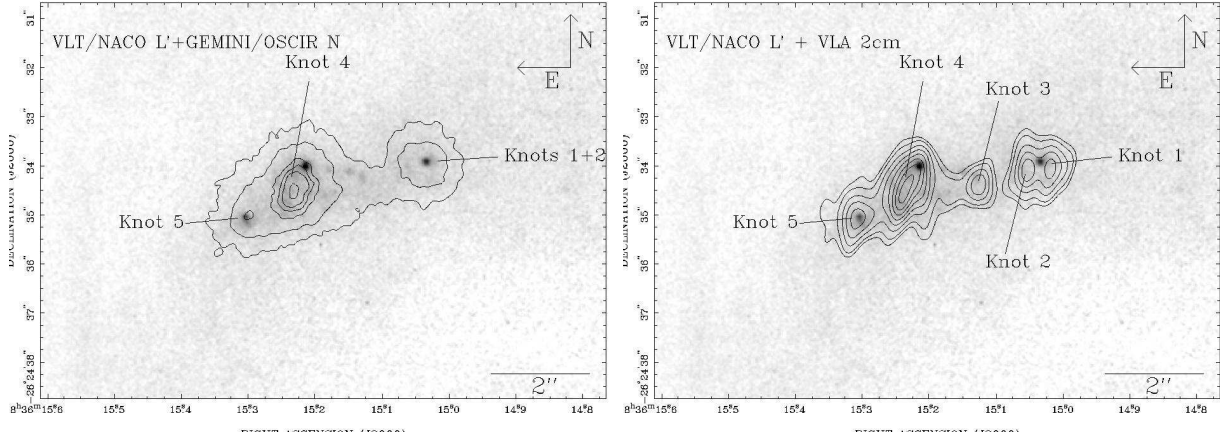


Fig. 4.— Left:  $L'$  gray-scale image overlotted with Gemini  $N$  contours. Right:  $L'$  gray-scale image overlotted with VLA 2-cm contours. The  $N$  gray are named using the identification of Vacca et al. (2002). The radio knots are named according to Kobulnicky & Johnson (1999). The brightest  $L'$  sources are named following the radio knots (cf. text and Fig. 2).

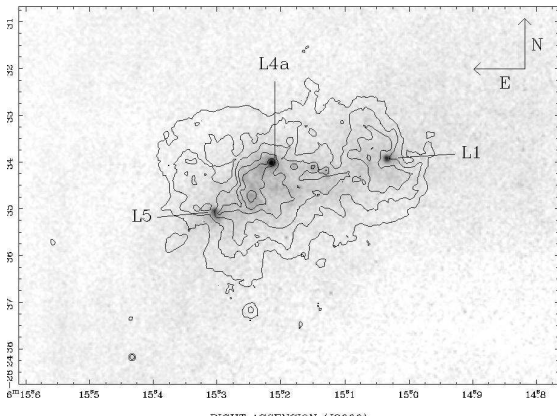


Fig. 5.— NACO  $L'$  gray-scale image overlotted with HST  $F658N/H\alpha$  contours.

faint source L2, we propose to associate the two sources L1 and L2 with knot 1 and knot 2 in the radio map. L2 has no counterpart in the optical bands, an anti-correlation with  $H\alpha$  (Fig. 5), much like L1, but is much fainter. Source L3a and L3b have clear optical and  $H\alpha$  counterparts west of the brightest optical source (cf. Fig. 5). They fall in a region of diffuse N-band emission and their association with knot 3 is unclear. The brightest  $L'$  source L4a is the counterpart of the main source in the F814W image. It is fainter in the  $H\alpha$  image but reappears strongly in the F555W image. Again L4a appears displaced from its possible radio and MIR counterpart knot 4. In fact it is quite likely that knot 4 and the associated brightest MIR source are the counterparts of the group L4b, c and d. These sources are easily detectable in the optical wide bands and are quite strong in  $H\alpha$ . L5 is another bright source that has no optical or  $H\alpha$  counterpart (Fig. 5) but is clearly detected in  $K_S$ , N and radio and can be associated with knot 5. L6 has no clear radio or MIR counterpart but is associated to the optical cluster just west of the brightest F814W source. Finally L7 and L8 have no definite counterparts but are associated with diffuse emission in all bands.

We emphasize that the fact that we detect spatially correlated sources across the spectrum doesn't mean that we actually detect the *same* sources. An error of  $0.2''$  translates to 9 pc at



He 2-10’s distance, while the compact sources are not expected to have sizes much larger than 1-2pc, hence the  $L'$  sources and radio knots could belong to contiguous yet distinct star forming regions. A robust identification will have to wait for deeper  $L'$  observations and higher resolution radio observations. Nevertheless, it is interesting to follow the working hypothesis that association between radio and NIR sources is indeed a physical one.

### 3.2. Near-infrared/optical colors of He 2-10 nucleus

We selected the sources likely to be clusters at 9 Mpc with a magnitude threshold of  $M_V < -8.5$  (Whitmore et al. 1999; Johnson et al. 2000). Table 2 shows the corresponding Vega magnitudes of the 12 central sources (Fig 2). All 12 sources seen in  $L'$  would still be too bright to be supergiant stars if Henize 2-10 was at a distance of 6 Mpc, but 2 sources out of the 21 outer sources detected in  $V$ ,  $I$  and  $K_S$  would fall below the threshold. We plot  $V - I$  vs  $V - K$ ,  $V - I$  vs  $I - L'$  and  $V - I$  vs  $K - L'$  colors in Figure 6 along with the dust free STARBURST99 (Leitherer et al. 1999, SB99) tracks of solar metallicity instantaneous bursts, with Salpeter IMF, from 0 (low  $V - I$ ) to 1 Gyr (high  $V - I$ ). The sharp turnoff seen in  $V - I$  vs  $K - L'$  correspond to 6.3 Myr, after which nebular emission ceases to be important. The 12 sources of the nucleus are plotted as squares the size of which relate to the total errors. The source of the outer  $1'$  are plotted as filled triangles for the sources belonging to the regions B and C of the north-east and west/north-west (Fig. 1), and as circles for sources falling at least  $1'$  away from the nucleus (all circles happen to be in the southern part of He 2-10, visible as bright blue [probably foreground] clusters in Fig. 1). Photometric errors are typically contained within the size of the symbol, but systematics related to the diffuse background subtraction can be of the order of 15%.

The solid arrows show the direction and the amplitude of a screen extinction of  $A_V = 1$  mag (assuming a Calzetti form instead of the canonical galactic extinction curve does not change the values by more than 3% in the range  $0.55 \mu\text{m}$ - $3.8 \mu\text{m}$ ). All diagrams show the well-known age-extinction degeneracy of optical colors (here  $V - I$ ), as well as the gradual decrease of the extinction impact on colors as one goes to the infrared. All show

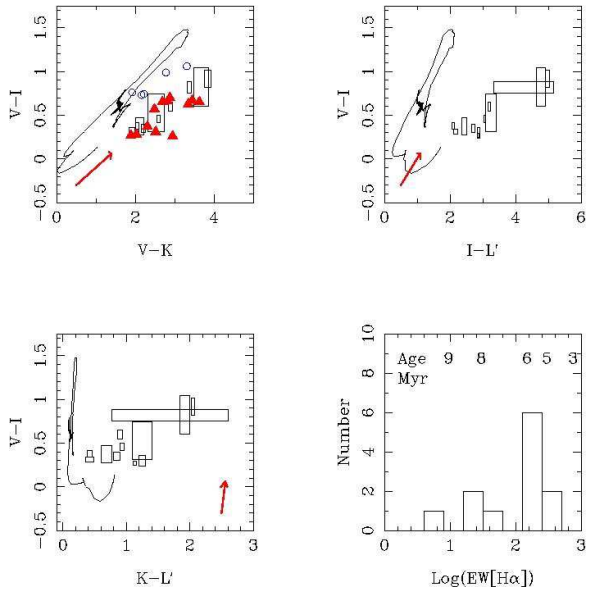


Fig. 6.— Color-color diagrams of all 12 sources detected in  $L'$  with VLT-NACO in Henize 2-10 central nucleus (squares; sizes proportional to errors), and of 21 sources visible in the VLT/ISAAC  $K_S$  covering the outer  $1'$  around the nucleus (open circles are for the most remote sources, filled triangles are sources surrounding the nucleus, mostly from so-called regions B and C). The outer sources are visible only up to  $K_S$  hence they are present only in the top-left diagram. Only sources brighter than  $M_V < -8.5$  are included.  $V$  and  $I$  magnitudes were extracted from HST archive images (cf. text). The thin solid lines are dust free STARBURST99 track of solar metallicity, Salpeter IMF of instantaneous bursts from 0-1Gyr (low  $V - I$  to high  $V - I$ ). The thick arrow shows the amplitude and direction of  $A_V = 1$  mag internal extinction. Bottom graph shows the  $H\alpha$  equivalent width ( $\text{Log}(\text{EW}[H\alpha])$ ) of the 12  $L'$  sources computed from an HST  $F658N$  archive image (cf. text).

that most of the data points cannot be explained by reddening any point of the models by any amount of screen extinction, especially for the diagrams including the  $L'$  photometry. This is a rather common observation in starburst regions (Johnson et al. 2004; Vanzi & Sauvage 2004; Cresci et al. 2005).

On the top left panel, the squares and the triangles seem to occupy the same locus whereas the circles are shifted up by  $V-I \simeq 0.3 \pm 0.1$  mag. This shift can be due to a systematic effect in the background subtraction although unlikely because the colors of triangles and squares were derived with independent methods (cf section 2.2) and still lies on top of each other, hence do not seem to be dominated by systematics. The shift more likely comes from an infrared excess affecting the central sources of He 2-10. This conclusion finds some support in the large excesses of  $I-L'$  and  $K-L'$  colors observed for the 12 central sources in the other two color-color diagrams. These infrared color excesses can have a number of explanations that will be explored later. But let us first characterize the magnitude of the extinction affecting the central sources. This will help us setting constraints on clusters ages as well as on their actual infrared excess from their location in the color-color diagrams.

As expected in a complex region such as revealed by Figure 1, extinctions measured at different wavelengths do not agree well with one another. First Allen et al. (1976) measure  $A_V=2.3$  from optical observations while Johansson (1987) correcting for the contribution of stellar absorption features obtain  $A_V = 0.86$ . Then we can use the observation of Vanzi & Rieke (1997) to derive the extinction of the central part of He 2-10 from the  $H\alpha$  to  $Br\gamma$  ratio. Vanzi & Rieke measure a  $Br\gamma$  flux of  $6.3 \times 10^{-14}$  erg.s $^{-1}$ .cm $^{-2}$  over an aperture of  $2.4 \times 15.6''$  centered on the K bright nucleus. From the HST  $H\alpha$  image we measure the  $H\alpha$  flux on the same aperture and obtain a value of  $1.86 \times 10^{-12}$  erg/s/cm $^2$ . Assuming an intrinsic  $H\alpha/Br\gamma$  ratio of 155.4 corresponding to  $T_e=7500$  K,  $n_e=1000$ cm $^{-3}$  (Storey & Hummer 1995) we find  $A_V = 1.25$ . Finally, from the ratio  $Br\gamma/Br10$  of Vanzi & Rieke we obtain  $A_V=10.5$  which is in full agreement with the extinction derived using the  $Br\alpha$ ,  $Br\gamma$  fluxes of Kawara et al. (1989). We thus observe a clear trend of increasing extinction from the optical to

the IR which is typical of a system where the absorbing material, gas and dust is mixed with emitting sources. It is worthwhile to note here that correcting the clusters for extinction will bring them closer to the youngest part of the SB99.

But this correction cannot explain the significant red excess observed in  $V-K$ ,  $I-L'$  and  $K-L'$  for all the central sources. This red excess was also observed in a similar diagram built for NGC 5253 (Vanzi & Sauvage 2004; Cresci et al. 2005) and for Haro 3 (Johnson et al. 2004), and most likely has the same origin: a contribution of hot dust in the NIR bands. Indeed as the earliest evolutionary phase of star clusters occurs deep in molecular clouds, we can expect to find dust and molecular clouds in the immediate vicinity of these clusters. Dust close to its sublimation temperature would be able to contaminate the  $L'$  band. Using radiative transfer models, Vanzi & Sauvage (2004) showed that the location of the reddest clusters in the  $(V-I, K-L')$  diagram of NGC 5253, could be explained by a combination of extinction, scattering and emission by dust in a shell around the cluster. This is likely what we observe here as well. In that respect, it is noteworthy that the three reddest sources in  $K-L'$  are L1, L2 and L5, the sources with no visible counterparts and associated with thermal radio knots. If we apply to the 12 central sources of He 2-10 color corrections such as those derived from the modeling of the red cluster in NGC 5253, this will bring all the sources to the bottom left of the diagrams, indicating ages of less than 6.3 Myr.

### 3.3. Physical properties

We study now the physical properties of the sources which dominates the  $L'$  emission of the nucleus (Fig. 2). The bright  $L'$  sources L1+L2, L4 and L5 are not or barely resolved with radii  $\sim 0.1''$  or 4.5 pc, L5 is not isolated, there is a faint diffuse emission extending as far as 3 FWHMs (10 pc) (the apertures shown on Fig. 2 are 22.5pc wide). These sources are not resolved in  $M'$  either (radii  $\lesssim 0.12''$ ). Fig.6 bottom panel shows the histogram of the  $H\alpha$  equivalent width  $\text{Log}(\text{EW}[H\alpha])$  of the 12 central sources in units of  $\text{Log}[\text{\AA}]$  (from Table 2) and the associated ages according to Leitherer & Heckman (1995). The histogram peaks at ages  $\lesssim 6$  Myr in agreement with recent works (Johnson et al. 2000; Chandar

et al. 2003) and with age trends inferred from previous section color analysis. We emphasize that the  $H\alpha$  equivalent width measurements are prone to strong systematic effects. We subtracted out the  $[NII] \lambda 6584$  measured to be 31% of  $H\alpha$  in an unpublished high-resolution spectrum covering the  $1.6''$  around source  $L4a$ . But the main source of error is a poorly-known continuum level. Our method to derive the continuum by interpolation of the contiguous broadband filters continuum for lack of a better estimator is crude and the quoted  $\text{Log}(\text{EW}[H\alpha])$  should be carefully used.

The measured  $\text{Log}(\text{EW}[H\alpha])$  centered on the sources L1, L2 and L5 are 2.60, 2.66 and 2.37, yielding ages  $\lesssim 5$  Myr. But the  $H\alpha$  emission shows remarkable anti-correlations with the source L1+2 and L5 and no emission in  $F555W$ ,  $F658N$  and  $F814W$  can be clearly associated with source L1, L2 and L5. Hence the measured  $\text{Log}(\text{EW}[H\alpha])$  is probably more related to He 2-10 foreground medium rather than the  $L'$  emitting clusters. An interesting check on the age derived from  $\text{Log}(\text{EW}[H\alpha])$  comes from the sources L3a, L3b, L4a and L6 because all three have unambiguous  $F555W$ ,  $F658N$  and  $F814W$  counterparts.  $\text{Log}(\text{EW}[H\alpha]) < 1.5$  and the brightest source in  $L'$  (L4a of Fig. 2) have  $\text{Log}(\text{EW}[H\alpha]) < 1.5$  (Table 2), consistent with the measurements of Johnson & Kobulnicky (2003, Fig. 9), yielding ages  $> 6$  Myr, whereas Chandar et al. (2003) derived ages of 4-5 Myr fitting single-burst SB99 templates to a dereddened UV/STIS spectrum of the same sources. Thus there appears to be an age dichotomy, with source L1, L2 and L5 being younger than 5 Myr and the other  $L'$  source being older.

On the basis of the new identification of the components across the spectrum (see Section 3.1), it is important to review previous assumptions on the nature of He 2-10 radio knots emission. The presence of UD HII in He 2-10 is primarily inferred from observed turnovers from flat radio spectra ( $F_\nu = \nu^{-\alpha}$  with  $\alpha = 0$ , characteristic of an optically thin ionized gas), to thermal spectra ( $\alpha = 2$ , signature of a free-free optically thick gas) (Kobulnicky & Johnson 1999). This feature is common in galactic HII regions. These UD HII regions were presumed to be extremely young, e.g. less than one million year, mostly because of their compactness, their high electron densities, and of their lack of counterpart in the

NIR and below. Indeed only HII regions buried extremely deep in dust, i.e. right at the start of their expansion, would remain invisible in the NIR. Since most of the radio sources now have counterparts, the interpretation of the radio knots must be updated.

Among the 5 radio sources, we would only classify knot 1+2 and knot 5, as bona fide UD HII regions. They have counterparts in the NIR but not in the visible. This implies a significant optical depth (typically  $\gtrsim 10$  if we follow existing models of embedded super-star clusters), and thus a young age although possibly not as young as previously postulated.

The radio knot 3 was already known to be a different type of source than other radio knots from a strong non-thermal signature Johnson & Kobulnicky (2003), (very likely a supernova remnant). We also propose that the radio knot 4, associated with diffuse  $L'$  emission (L4b,c,d) and showing strong correlations with bright optical and  $H\alpha$  sources, is not an UD HII region but a complex mix of *normal* HII regions and supernova remnants. Knot 4 does show a non-thermal signature with a slightly negative spectral index  $\alpha$ . The proposed re-classification of the radio sources would lower the total mass of hidden  $O$  stars (as deduced from the radio) by a factor of  $\sim 2$  Johnson & Kobulnicky (2003).

Detailed modelling of the spectral energy distributions is essential to have a deeper understanding of the star formation process ongoing in He 2-10, especially of sources L1+L2 and L5 which represent the best candidate for very young dust-enshrouded super-star clusters. This is however a long endeavour that we defer to a later paper. Nevertheless the present observations outline the importance of high-resolution multiwavelength datasets to disentangle the intrinsically complex nature of star forming regions.

#### 4. Conclusions

We detected compact sources in the nucleus of Henize 2-10 with  $K_S$ ,  $L'$  and  $M'$  observations using ISAAC and NAOS-CONICA on the VLT. The sources are compact ( $< 4.5$  pc), highly correlated with radio and mid-infrared ultradense HII regions, previously thought to be optically thick.

The color-color magnitude diagrams show the

presence of strong red-excess in  $K_S$  and  $L'$ . Such red excesses point at highly heterogeneous dust distribution and at the presence of a hot dust component emitting and scattering down to  $L'$  and  $M'$ .

We tentatively review the previous classification of the radio knots by identifying two bona fide UD HII (knot 1+2 and knot 5) and propose that knots 3 and 4 are non-thermal radio sources, akin to supernova remnants.

These new high-resolution data uncover a complex structure in infrared. We suggest that to understand He 2-10 star forming history, a detailed model of the radiative processes is needed. This model should include all known components of the galaxy in a consistent way in order to fit the spectral energy distribution from radio to UV.

RAC wish to acknowledge an ESO grant for visiting scientist in Santiago, and thank Chip Kobulnicky for sharing his VLA 2-cm data and Kelsey Johnson for useful comment on the first version of the paper.

Facilities: VLT(ISAAC) VLT(NAOS-CONICA)

## REFERENCES

- Allen, D. A., Wright, A. E., & Goss, W. M. 1976, *MNRAS*, 177, 91
- Beck, S. C., Turner, J. L., & Gorjian, V. 2001, *AJ*, 122, 1365
- Chandar, R., Leitherer, C., Tremonti, C., & Calzetti, D. 2003, *ApJ*, 586, 939
- Cresci, G., Vanzi, L., & Sauvage, M. 2005, *A&A*, 433, 447
- Holtzman, J. A., Burrows, C. J., Casertano, S., Hester, J. J., Trauger, J. T., Watson, A. M., & Worthey, G. 1995, *PASP*, 107, 1065
- Hutsemekers, D., & Surdej, J. 1984, *A&A*, 133, 209
- Johansson, I. 1987, *A&A*, 182, 179
- Johnson, K. E., & Kobulnicky, H. A. 2003, *ApJ*, 597, 923
- Johnson, K. E., Leitherer, C., Vacca, W. D., & Conti, P. S. 2000, *AJ*, 120, 1273
- Johnson, K. E., Indebetouw, R., Watson, C., & Kobulnicky, H. A., 2004, *AJ*, 128, 610
- Kawara, K., Nishida, M., & Phillips, M. M. 1989, *ApJ*, 337, 230
- Kobulnicky, H. A., & Johnson, K. E. 1999, *ApJ*, 527, 154
- . 2000, *ApJ*, 539, 1023
- Kobulnicky, H. A., Kennicutt, R. C., & Pizagno, J. L. 1999, *ApJ*, 514, 544
- Leitherer, C., & Heckman, T. M. 1995, *ApJS*, 96, 9
- Leitherer, C., Schaerer, D., Goldader, J. D., Delgado, R. M. G., Robert, C., Kune, D. F., de Mello, D. F., Devost, D., & Heckman, T. M. 1999, *ApJS*, 123, 3
- Monet, D. B. A., Canzian, B., Dahn, C., Guetter, H., Harris, H., Henden, A., Levine, S., Luginbuhl, C., Monet, A. K. B., Rhodes, A., Rieke, B., Sell, S., Stone, R., Vrba, F., & Walker, R. 1998, *VizieR Online Data Catalog*, 1252, 0
- Sauvage, M., Thuan, T. X., & Lagage, P. O. 1997, *A&A*, 325, 98
- Schlegel, D. J., Finkbeiner, D. P., & Davis, M. 1998, *ApJ*, 500, 525
- Storey, P. J., & Hummer, D. G. 1995, *MNRAS*, 272, 41
- Tully, R. B. 1988, *Nearby galaxies catalog* (Cambridge and New York, Cambridge University Press, 1988, 221 p.)
- Vacca, W. D., & Conti, P. S. 1992, *ApJ*, 401, 543
- Vacca, W. D., Johnson, K. E., & Conti, P. S. 2002, *AJ*, 123, 772
- Vanzi, L., & Rieke, G. H. 1997, *ApJ*, 479, 694
- Vanzi, L., & Sauvage, M. 2004, *A&A*, 415, 509
- Whitmore, B. C., Zhang, Q., Leitherer, C., Fall, S. M., Schweizer, F., & Miller, B. W. 1999, *AJ*, 118, 1551